ChemComm

COMMUNICATION

View Article Online
View Journal | View Issue

Cite this: *Chem. Commun.*, 2015, **51**, 9535

Received 12th February 2015,
Accepted 21st April 2015

DOI: 10.1039/c5cc01316j

www.rsc.org/chemcomm

Structure transition of Au_{18} from pyramidal to a hollow-cage during soft-landing onto a TiO_2(110) surface†

Lei Li,[a] Hui Li[b] and Xiao Cheng Zeng*[a]

Au_{18} is a unique gold cluster in that, in the gas phase, two distinct isomers, namely, golden hollow-cage and golden pyramid, can coexist (*ACS Nano*, 2009, 3, 1225). We perform a Born–Oppenheimer molecular dynamics (BOMD) simulation to confirm the structural stability of the two isomers at ambient temperature. Most importantly, we study the possible structure conversion between the two isomers when they are soft-landed onto a rutile TiO_2(110) surface. Our BOMD simulation indicates that the Au_{18} cluster can undergo a transition from pyramidal to a hollow-cage structure during soft landing onto the rutile TiO_2(110) surface at ambient temperature, suggesting the high selectivity of the hollow-cage structure over the pyramidal structure in realistic soft-landing experiments.

Au clusters and nanoparticles have been intensively studied due to their exceptional catalytic activity towards numerous reactions, including CO oxidation,[1–6] thiophenol oxidation, propylene epoxidation[7] and the water-gas shift reactions.[8,9] One feature focused on in experimental and theoretical studies has been the size- and structure-dependent catalytic activity of Au clusters with or without metal-oxide support. It has been recognized that the catalytic activity of supported Au clusters can be strongly correlated with the local structure at the Au–TiO_2 interface. In reality, however, the local structure at the Au/support interface depends on the kinetically relaxed structure of the Au cluster after landing or growing on the support, or on the preparation method and environmental conditions. One experimental approach that has been used to prepare precisely controlled Au cluster/support systems for nanocatalysis studies is the so-called soft-landing, in which the clusters are size-selected through mass spectrometry.[10–15] During the soft landing process, structural deformation of the Au clusters may occur after collision with the support.[15,16] Significant structural deformation may dramatically affect the contact area between the Au clusters and the support, thereby leading to different catalytic activities. *Ab initio* molecular dynamic simulation of the soft-landing process of sub-nanometer gold clusters not only allows us to monitor the time-dependent structure evolution of the Au clusters on the surface of the metal oxide support but also allows us to assess the structural stability and possible structure transition of different isomers at different temperatures.

In a recent study, we have shown the high catalytic activity of the hollow-cage Au_{18} ($Au_{18\text{-cage}}$) cluster soft-landed onto a rutile TiO_2(110) surface, as well as the high structural stability of the hollow-cage Au_{18} cluster during collision with the rutile TiO_2(110) surface or in the reaction environment of CO oxidation.[16] Nevertheless, besides the hollow-cage isomer, the pyramidal isomer ($Au_{18\text{-pyrd}}$) is another abundant isomer in gas phase reactions although it is much less active towards CO oxidation.[16–19] From the standpoint of increasing the catalytic activity, it would be desirable to convert the pyramidal isomer to the hollow-cage isomer for Au_{18}. To explore this possibility, we simulate the soft-landing process of $Au_{18\text{-pyrd}}$ onto the rutile TiO_2(110) surface. Interestingly, our BOMD simulation shows that the structural transition of Au_{18} from pyramidal to the hollow-cage can occur during the soft-landing process onto the rutile TiO_2(110) surface at room temperature.

Our BOMD simulation is performed on the basis of the density functional theory method in the form of Perdew–Burke–Ernzerhof (PBE) functional, implemented in the CP2K code.[20–22] A mixed Gaussian and plane-wave (GPW) basis set with the Goedecker–Teter–Hutter (GTH) pseudopotential is adopted to treat the interaction between the core and valence electrons.[21,22] The plane-wave energy cutoff is set as 280 Ry. The energy convergence is set to 1.0×10^{-7} a.u. so that the total energy drift does not exceed 0.67% of the initial kinetic energy per picosecond (ESI,† Fig. S1). A (110)-terminated rutile TiO_2 slab (6×3) is used to model the TiO_2 surface.

[a] *Department of Chemistry, University of Nebraska-Lincoln, Lincoln, NE 68588, USA. E-mail: xzeng1@unl.edu*
[b] *Institute of Physics, Chinese Academy of Sciences, Beijing, 100190, China*

† Electronic supplementary information (ESI) available: Time-evolution of the total energy and a video of the trajectory of the BOMD simulation for simulating the soft-landing of the Au_{18} cluster onto a TiO_2(110) surface, snapshot structures, the corresponding time-evolution of R^{min}_{Au-COM}, the $g(r)$ functions of the Au–COM distance for the second and the third BOMD simulations Run 2 and 3, videos of the trajectories of the thermal stability test of the pyramidal and the hollow-cage Au_{18} clusters, and coordinates of the optimized clusters on the TiO_2 surface. See DOI: 10.1039/c5cc01316j

The slab contains 12 atomic layers with the top six atomic layers free to relax while the bottom six atomic layers are fixed at their lattice position. To simulate the soft-landing process, a neutral $Au_{18\text{-pyrd}}$ cluster is initially located ~5.0 Å above the rutile TiO_2(110) surface so that only weak dispersion interaction exists between the Au cluster and the rutile TiO_2(110) surface. The initial thermal velocities of the atoms of the Au cluster and the top 6 atomic layers of the TiO_2 substrate are given based on the Boltzmann distribution at 298 K. Then, the velocities of the Au atoms along the z direction (perpendicular to the rutile TiO_2(110) surface) are reset so that the initial relative velocity (v_z) between the Au cluster and the TiO_2 support is ~207 m s^{-1}. The sum of the thermal kinetic energy and translation kinetic energy of the Au cluster amounts to ~0.1 eV per atom, satisfying the soft-landing conditions (in experiments, the kinetic energy in the range of 0.02 to 0.2 eV per atom is typically used for soft landing of nanoparticles onto hard surfaces, *i.e.*, oxide surface).[12,13,23–27] In the size-selection step involved in all soft-landing experiments, the Au clusters must carry a charge.[27,28] It is expected that during the soft-landing, the charge would be lost to the support, leaving the charge of the Au clusters neutral.[29,30] Hence, in our simulation, the neutral Au cluster is selected. The BOMD simulation is performed in the constant-energy, constant-volume (*NVE*) ensemble with a timestep of 1.0 fs.

Snapshots at several stages of the BOMD simulation, time-evolution of the Kohn–Sham (KS) energy and the temperature of the Au_{18}/TiO_2 system are displayed in Fig. 1. As shown in Fig. 1a, energy conversion from the kinetic energy to KS potential energy can be seen in the following three time intervals: collision period (~1–4 ps), structure transition period (~18–27 ps), and post-transition period (>27 ps). In the collision period, the Au_{18} cluster starts to collide with the TiO_2 surface at ~1 ps and structural deformation is induced. During this period, the temperature decreases first and then increases while the KS potential energy increases first and then decreases. The structure of Au_{18} continues to evolve due to the deformation. At ~20 ps, the potential energy starts to increase with a concomitant decrease in the temperature. Such energy conversion corresponds to the structure transition of the Au cluster to the hollow-cage structure. The increase in the KS potential energy manifests the climbing of the energy barrier that is required to complete the structure transition from pyramidal to the hollow-cage. Upon the structure transition, the Au_{18} cluster starts to shift along the (100) direction and even flips over on the TiO_2 surface (ESI,† Movie S1), manifested by post fluctuation of the KS energy and the kinetic energy. Subsequently, no further structure deformation is observed upon the formation of the hollow-cage structure at ~27 ps, indicating the higher stability of the hollow-cage Au_{18} isomer over the pyramidal isomer after the soft landing.

To further confirm the occurrence of the structure transition, we calculate the minimum distance of the Au atom that is closest to the center of the mass (COM) of the Au_{18} cluster, and the number of Au atoms within 2.40 Å of the COM of the Au_{18} cluster at each time step during the BOMD simulation. The two quantities are denoted as R^{min}_{Au-COM} and $N^{R<2.40}_{Au}$, respectively, as shown in Fig. 2. Before the structure transition (<18 ps), R^{min}_{Au-COM} fluctuates around the average value ~1.75 Å with a relatively large fluctuation range (from ~1.10 to 2.40 Å) due to the structure deformation induced by the collision. Beyond 18 ps, the mean value of R^{min}_{Au-COM} starts to increase and reaches ~2.40 Å at ~21 ps. Beyond 21 ps, R^{min}_{Au-COM} mainly fluctuates around ~2.40 Å and the amplitude of the fluctuation becomes gradually smaller, implying that a relatively stable structure is attained. Furthermore, the time variation of $N^{R<2.40}_{Au}$ describes the dynamic behavior of the Au atoms near the core area within a radius of ~2.40 Å. As shown in the lower panel of Fig. 2, before the collision (t < 1 ps), $N^{R<2.40}_{Au}$ is about 4, indicating that four Au atoms are favored to stay in the core region, corresponding to the existence of the four facet atoms (yellow atoms in Fig. 3(b) upper panel) in the $Au_{18\text{-pyrd}}$. From 1 to ~18 ps, $N^{R<2.40}_{Au}$ starts to fluctuate between 1 and 4, with an average value of ~2, suggesting a relatively high probability of finding the Au atoms in the core region. After the structure transition (t > 21 ps), the number of Au atoms in the core region is not more than 2, and sometimes there are no Au atoms in this region. In other words,

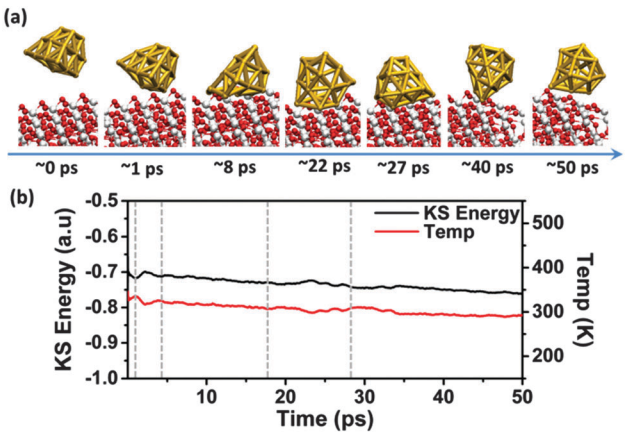

Fig. 1 (a) Snapshots at several time intervals from the BOMD simulation of the soft-landing process of Au_{18} onto the rutile TiO_2(110) surface. (b) Time-evolution of the temperature and Kohn–Sham energy of the Au_{18}/TiO_2 system during the soft-landing process. The dashed gray lines mark the time at 1, 4, 18 and 27 ps, respectively.

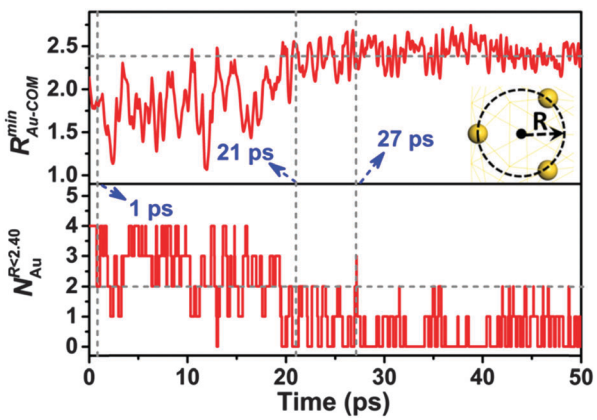

Fig. 2 The upper panel displays the time evolution of the minimum distance of the Au atom that is closest to the center of mass (COM) of the Au_{18} cluster (R^{min}_{Au-COM}). The lower panel displays the number of Au atoms that are within a radius of ~2.40 Å about the COM of the Au_{18} ($N^{R<2.40}_{Au}$).

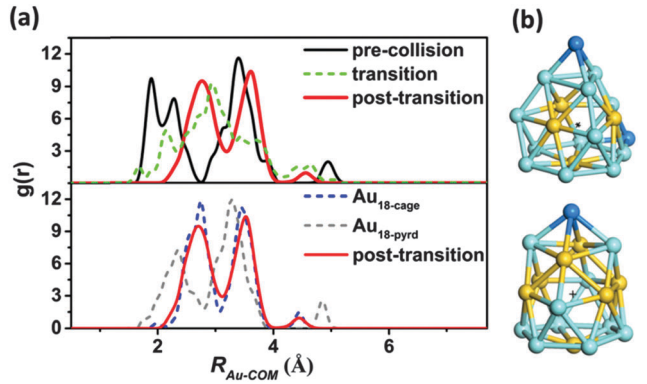

Fig. 3 (a) The upper panel depicts the radial distribution functions ($g(r)$) of the Au–COM distance for three typical time stages: pre-collision (black line, $t < 1$ ps), structure transition (green dashed line, 18 ps $< t <$ 27 ps) and post-transition (red line, $t > 27$ ps). The comparison of the $g(r)$ functions of the Au–COM distance in the post-transition period with that of a bare $Au_{18\text{-cage}}$ (dashed blue lines) and $Au_{18\text{-pyrd}}$ (dashed gray line) is shown in the lower panel. (b) The optimized structures of $Au_{18\text{-pyrd}}$ (upper panel) and $Au_{18\text{-cage}}$ (lower panel). The yellow, light blue and dark blue spheres represent the Au atoms in the inner, middle, and outer shell respective to the COM of the Au cluster, respectively.

the probability of the Au atoms appearing in the core region ($r < 2.40$ Å) is greatly reduced. To summarize, the increment of $R^{\min}_{\text{Au–COM}}$ results in an enlargement of the empty core region rarely occupied by the Au atoms, indicating the formation of a cage-like structure.

For the purpose of comparison, we performed a BOMD simulation to compute the radial distribution functions ($g(r)$) of the Au–COM distance for both the hollow-cage and pyramidal Au_{18} clusters in the gas phase (see Fig. 3). The simulation was carried out in the constant-volume and -temperature (*NVT*) ensemble with the temperature controlled at ~300 K. As shown in the ESI,† movies S2 and S3, both gas-phase Au_{18} isomers can maintain their original structures with little structure deformation at least within 20 ps of the BOMD simulation, indicating the thermal stability of both gas-phase clusters. In their $g(r)$ functions, three main peaks are observed, which are corresponding to the inner-, middle- and outer-shell Au atoms, respectively, as depicted in Fig. 3b. In Fig. 3a, we also plot computed radial distribution functions $g(r)$ of the Au–COM distance over three time periods: the pre-collision period ($t < 1$ ps), the structure-transition period (18 ps $< t <$ 27 ps), and the post-transition period ($t > 27$ ps). Comparison of the three $g(r)$ functions illustrates the structure evolution of the Au_{18} cluster during the soft-landing process. Before the collision, three peaks are located at ~1.846, ~3.315 and ~4.822 Å. These peaks are mostly consistent with those shown in the $g(r)$ of the bare $Au_{18\text{-pyrd}}$ cluster, although the long-range interaction between the Au_{18} cluster and the rutile $TiO_2(110)$ surface results in splitting and left shifting of the first peak. The structure deformation induced by the collision leads to the outer-shell shifting of Au atoms as reflected by the lowered first peak from the pre-collision to the structure transition stage. As a result, the $g(r)$ in the structure transition stage shows structural features of both the $Au_{18\text{-pyrd}}$ and $Au_{18\text{-cage}}$ clusters. In the post-transition stage, the peak at ~1.846 Å disappears. Instead, a peak at ~2.749 Å is seen. This apparent shifting of the first peak to a longer distance by ~0.903 Å signifies expansion of the empty core region with the radius increasing from ~1.741 to ~2.413 Å (the values are taken from the half-height positions of the first peak). On the contrary, the peak originally located at ~4.822 Å is lowered by half in height, and shifts to a shorter-distance range. This results from the disappearance and the inner-shell shifting of the two corner-atoms in the pyramidal structure (blue Au atoms in Fig. 3b). Such changes result in a good agreement between the $g(r)$ of the Au–COM distance with that of the bare $Au_{18\text{-cage}}$ cluster, confirming the formation of a hollow-cage structure in the post transition period. Here, the variation of the $g(r)$ function of the Au–COM distance illustrates the structure evolution of the Au_{18} cluster from the pyramidal to the hollow-cage structure during the soft-landing process.

To understand the origin of the transition from the pyramidal to the hollow-cage structure, we have computed the time evolution of the total energy of the Au_{18} cluster during the soft-landing process (Fig. 4). From the energy evolution of the Au_{18} cluster, an energy barrier is seen from the pyramidal to the hollow-cage structure. The collision between the Au_{18} cluster and the rutile $TiO_2(110)$ surface assists the surmounting of this energy barrier to trigger the structure transition. In addition, the Mulliken charge analysis indicates that the Au_{18} cluster is positively charged during 2–16 ps due to electron transfer from Au to the surface oxygen atoms. Our DFT calculation shows that the pyramidal Au_{18} cluster with a positive charge is less stable than the positively charged hollow-cage Au_{18} cluster by ~0.15 eV in energy. In other words, the electron transfer from the Au cluster to the TiO_2 surface can also destabilize the pyramidal Au_{18} cluster. Hence, the observed structure transition is likely resulted from a combined effect of the collision and the charge transfer between the Au_{18} cluster and the TiO_2 surface.

To further confirm the pyramid-to-cage transition, another two independent BOMD simulations (denoted as Run 2 and Run 3)

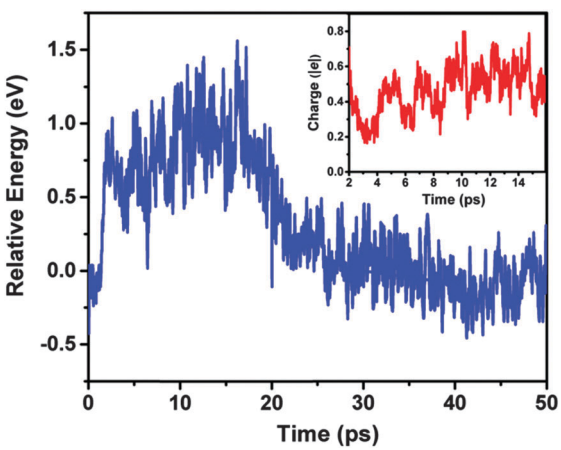

Fig. 4 Energy evolution of the Au_{18} cluster during the soft-landing process (from BOMD simulation, Run-1). The energy of the initial structure (pyramidal structure) of Au_{18} is set as 0. The inset image illustrates the Mulliken charge analysis of the Au_{18} cluster from 2 ps to 16 ps.

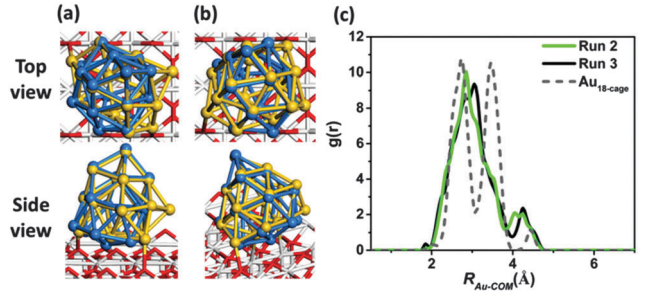

Fig. 5 (a) and (b) The optimized structures (yellow spheres) obtained from the second and the third BOMD simulation (Run 2 and Run 3, respectively) of the soft-landing of Au_{18} onto the rutile TiO_2(110) surface. The dark blue spheres represent the structure of the bare $Au_{18\text{-cage}}$ clusters. The corresponding $g(r)$ functions of the Au–COM distance for the post-transition period are presented in (c).

of the soft-landing of the pyramidal Au_{18} onto the rutile TiO_2(110) surface were performed. As shown in the ESI,† Fig. S2, a relatively stable structure is seen at ~30 and ~35 ps for Run 2 and Run 3, respectively. Our simulations indicate that the stable structure seen in both BOMD runs is the distorted hollow-cage structure (see Fig. 5a). The time-evolution of R^{min}_{Au-COM} for both BOMD runs indicates expansion of the empty core region from ~1.75 to 2.40 Å (ESI,† Fig. S2c). A comparison of $g(r)$ of the Au–COM distance for the pre-collision ($t < 1$ ps, ESI,† Fig. S3) and post-transition period ($t > 30$ and 35 ps for both Run 2 and Run 3; see Fig. 5c) suggests that the Au atoms tend to shift to the outer shell. Such an outer-shell shifting behavior is consistent with the formation of an empty core region with a radius of ~2.435 Å, and with the time evolution of R^{min}_{Au-COM}. As shown in both runs, collision of the Au_{18} cluster with the rutile TiO_2(110) surface leads to the formation of a hollow-cage structure.

As aforementioned, the pyramidal and hollow-cage structures are the two dominant structures for the mass-spectrometry selected Au_{18} clusters in the gas phase. Our previous study had shown that the hollow-cage Au_{18} cluster exhibits a much higher catalytic activity towards CO oxidation than the pyramidal isomer.[16] Also, the BOMD simulations have demonstrated that the hollow-cage isomer can maintain its structure not only during the soft-landing process, but also in the reaction environment of CO oxidation. Hence, in realistic soft-landing experiments involving Au_{18} clusters, the hollow-cage isomer is expected to be the most popular isomer and should play a dominant role in the high catalytic activity of the rutile TiO_2(110) supported Au_{18} clusters.

In conclusion, we have simulated the soft-landing process of pyramidal Au_{18} onto the rutile TiO_2(110) surface by using the large-scale BOMD simulations. All three independent BOMD simulations show that collision of the Au_{18} clusters with the TiO_2 surface leads to the outer-shell shifting of the Au atoms, thus resulting in the formation of a hollow-cage structure. Such a structure transition from the pyramidal isomer to the hollow-cage isomer indicates that the Au_{18} clusters tend to exhibit the hollow-cage structure after soft-landing onto the rutile TiO_2(110) surface. In view of the higher catalytic activity of the hollow-cage Au_{18} clusters, the conversion of the pyramidal isomer to the hollow-cage isomer through soft-landing is quite desirable. Our simulation also suggests that the size selection through mass-spectrometry combined with soft-landing of the Au clusters on the rutile TiO_2(110) surface offers an effective experimental approach for isomer-specific nanocatalysis studies.

Notes and references

1 M. Haruta, T. Kobayashi, H. Sano and N. Yamada, *Chem. Lett.*, 1987, 405–408.
2 M. Valden, X. Lai and D. W. Goodman, *Science*, 1998, **281**, 1647–1650.
3 M. Haruta, N. Yamada, T. Kobayashi and S. Iijima, *J. Catal.*, 1989, **115**, 301–309.
4 X. W. Xie, Y. Li, Z. Q. Liu, M. Haruta and W. J. Shen, *Nature*, 2009, **458**, 746–749.
5 N. Weiher, A. M. Beesley, N. Tsapatsaris, L. Delannoy, C. Louis, J. A. van Bokhoven and S. L. M. Schroeder, *J. Am. Chem. Soc.*, 2007, **129**, 2240–2241.
6 C. Y. Liu, Y. Z. Tan, S. S. Lin, H. Li, X. J. Wu, L. Li, Y. Pei and X. C. Zeng, *J. Am. Chem. Soc.*, 2013, **135**, 2583–2595.
7 T. Hayashi, K. Tanaka and M. Haruta, *J. Catal.*, 1998, **178**, 566–575.
8 F. Boccuzzi, A. Chiorino, M. Manzoli, D. Andreeva and T. Tabakova, *J. Catal.*, 1999, **188**, 176–185.
9 W. D. Williams, M. Shekhar, W. S. Lee, V. Kispersky, W. N. Delgass, F. H. Ribeiro, S. M. Kim, E. A. Stach, J. T. Miller and L. F. Allard, *J. Am. Chem. Soc.*, 2010, **132**, 14018–14020.
10 S. A. Miller, H. Luo, S. J. Pachuta and R. G. Cooks, *Science*, 1997, **275**, 1447–1450.
11 S. S. Lee, C. Y. Fan, T. P. Wu and S. L. Anderson, *J. Am. Chem. Soc.*, 2004, **126**, 5682–5683.
12 G. E. Johnson, T. Priest and J. Laskin, *ACS Nano*, 2012, **6**, 573–582.
13 G. E. Johnson, C. Wang, T. Priest and J. Laskin, *Anal. Chem.*, 2011, **83**, 8069–8072.
14 Z. W. Wang and R. E. Palmer, *Nanoscale*, 2012, **4**, 4947–4949.
15 H. Li, Y. Pei and X. C. Zeng, *J. Chem. Phys.*, 2010, **133**, 134707.
16 L. Li, Y. Gao, H. Li, Y. Zhao, Y. Pei, Z. F. Chen and X. C. Zeng, *J. Am. Chem. Soc.*, 2013, **135**, 19336–19346.
17 W. Huang, S. Bulusu, R. Pal, X. C. Zeng and L. S. Wang, *ACS Nano*, 2009, **3**, 1225–1230.
18 S. Bulusu and X. C. Zeng, *J. Chem. Phys.*, 2006, **125**, 154303.
19 S. Bulusu, X. Li, L. S. Wang and X. C. Zeng, *Proc. Natl. Acad. Sci. U. S. A.*, 2006, **103**, 8326–8330.
20 J. P. Perdew, K. Burke and M. Ernzerhof, *Phys. Rev. Lett.*, 1996, **77**, 3865–3868.
21 C. Hartwigsen, S. Goedecker and J. Hutter, *Phys. Rev. B: Condens. Matter Mater. Phys.*, 1998, **58**, 3641–3662.
22 S. Goedecker, M. Teter and J. Hutter, *Phys. Rev. B: Condens. Matter Mater. Phys.*, 1996, **54**, 1703–1710.
23 H. Haberland, M. Mall, M. Moseler, Y. Qiang, T. Reiners and Y. Thurner, *J. Vac. Sci. Technol., A*, 1994, **12**, 2925–2930.
24 S. H. Baker, S. C. Thornton, K. W. Edmonds, M. J. Maher, C. Norris and C. Binns, *Rev. Sci. Instrum.*, 2000, **71**, 3178–3183.
25 D. C. Lim, R. Dietsche, M. Bubek, G. Gantefor and Y. D. Kim, *ChemPhysChem*, 2006, **7**, 1909–1911.
26 R. Dietsche, D. C. Lim, M. Bubek, I. Lopez-Salido, G. Gantefoer and Y. D. Kim, *Appl. Phys. A: Mater. Sci. Process.*, 2008, **90**, 395–398.
27 W. P. Peng, M. P. Goodwin, Z. X. Nie, M. Volny, O. Y. Zheng and R. G. Cooks, *Anal. Chem.*, 2008, **80**, 6640–6649.
28 Z. X. Nie, G. T. Li, M. P. Goodwin, L. Gao, J. Cyriac and R. G. Cooks, *J. Am. Soc. Mass Spectrom.*, 2009, **20**, 949–956.
29 J. Laskin, P. Wang and O. Hadjar, *J. Phys. Chem. C*, 2010, **114**, 5305–5311.
30 G. E. Johnson and J. Laskin, *Chem. – Eur. J.*, 2010, **16**, 14433–14438.

